Electronic spectroscopy of fluorobenzene Van der Waals molecules by resonant two-photon ionization

ARTICLE *in* CHEMICAL PHYSICS · OCTOBER 1983

Impact Factor: 1.65 · DOI: 10.1016/0301-0104(83)85174-X

Chemical Physics 80 (1983) 129–145
North-Holland Publishing Company

ELECTRONIC SPECTROSCOPY OF FLUOROBENZENE VAN DER WAALS MOLECULES BY RESONANT TWO-PHOTON IONIZATION

K. RADEMANN, B. BRUTSCHY and H. BAUMGÄRTEL

Institut für Physikalische Chemie der Freien Universität Berlin, 1000 Berlin 33, Takustrasse 3, West Germany

Received 1 March 1983

Van der Waals (vdW) clusters of fluorobenzene (FB), synthesized in a seeded supersonic rare-gas expansion were studied by laser-induced, resonant two-photon ionization (R2PI) combined with TOF-mass spectrometry. The molecules were excited near the FB monomer's vibronic origin of the $S_1(\pi\pi^*) \leftarrow S_0$ transition ($\lambda_{00} = 2644$ Å). The heterogeneous clusters FB·Ar_n ($n < 4$) showed specific shifts of the 0–0 band relative to λ_{00} induced by vdW interaction (FB·Ar: -23 cm^{-1}; FB·Ar_2: -46 cm^{-1}; FB·Ar_3: $+4.6$ cm^{-1}). Additional satellite bands appeared due to intermolecular photofragmentation. A second band found for FB·Ar at 20 cm^{-1} was assigned to a vdW vibration ($\nu_{vdW} = 43$ cm^{-1}). Similar results were obtained for FB·Kr_n ($n < 3$). The spectra of the homogeneous clusters FB_2 and FB_3 were more complex. The dimer spectrum showed two broad spectral features, one blue- the other red-shifted relative to λ_{00}. Each one is probably due to a different isomer. The blue-shifted contained progressions, which were tentatively assigned to a vdW vibration with 20 cm^{-1} in the ground and 15 cm^{-1} in the excited state. The trimer spectrum showed a broad blue-shifted absorption maximum with prominent bands at -2.6, -20, -29 and -50 cm^{-1}.From the observed spectra the feasibility of cluster-specific spectroscopy is discussed.

1. Introduction

The structure, energetics and intramolecular dynamics of vdW clusters are of considerable importance for the basic understanding of intermolecular interaction in chemistry [1–3]. The stepwise study of molecular properties going from the isolated molecule to the condensed phase is, for instance, relevant to understanding homogeneous nucleation [4] and catalysis phenomena [5]. Most experimental work done on vdW clusters from a microscopic point of view may be subdivided into three categories of spectroscopy. Namely, (1) the IR [6,7] and RF-electric resonance [8,9] spectroscopy for studying the structure, energetics and dynamics of the weakly-bound ground state of the neutral vdW molecules ($E_{DIS} \approx 10$–500 cm^{-1}); (2) the photoionization mass spectroscopy with VUV-light for the determination of the features of ionic clusters [10–17] and (3) the optical spectroscopy by laser-induced fluorescence (LIF) [18–23] for the elucidation of the excited-state energetics and dynamics. A synthesis of the last two methods is the study of vdW clusters by resonant two-photon ionization (R2PI) with tunable lasers [24–30]. Normally the first step of this two-step ionization is resonant with an electronically excited state, the second step is generally not resonant, leading into the ionization continuum. Up to the present, most spectroscopic work in this field was done with two photons of one color (1C-R2PI). In this case, the energy of the resonant state is more than half of the ionization limit. From the experimental point of view the excited state should lie in an energy range accessible by modern pulsed dye lasers combined with frequency doubling ($\lambda = 217$–300 nm). In the past, for these two reasons, mainly aromatic or metal clusters [34] have been investigated.

The R2PI spectrum, i.e., the ion intensity as a function of the laser wavelength, reflects the resonant structure of the excited state. With two separately tunable lasers two-color R2PI (2C-R2PI) is possible. In this case the energy of one photon is resonant with an electronically excited state, while

0301-0104/83/0000–0000/$03.00

the energy of the other photon can be varied to measure ionization and fragmentation appearance potentials with very high accuracy [28,29]. Few experiments so far were done with 2C-R2PI of organic vdW clusters, mainly those of the Smalley [29,30] and Schlag [28] groups.

The reasons that make R2PI such an attractive method for the spectroscopy of vdW clusters are the following [35]. The basic problem in studying clusters synthesized in a supersonic expansion is the fact that it is generally not possible to produce a specific cluster size. More often a broad distribution of clusters (with different sizes but similar spectral properties) is found in the beam. Due to the weakness of the vdW interaction all spectroscopy done by excitation or ionization of the molecules may be complicated by fragmentation. Dehmer and Pratt [15] only recently showed that ion-yield curves of Ar_3^+ measured in one-photon ionization mass spectroscopy (even close to the ionization limit) depend strongly on the source conditions. This observation can only be explained by simultaneous fragmentation of larger clusters, resulting in the same ionic product, Ar_3^+. Fragmentation, for example by vibrational or rotational predissociation [3] of the ions, may explain that ion-yield curves of large clusters show in general only a very smeared out structure [10,11,14]. Therefore a method for the photoionization mass spectroscopy of clusters which is softer and more mass-selective is a prerequisite in studying features of a specific cluster. Due to the high intensity and monochromaticity of lasers R2PI has proved to be a very mass-selective and sensitive method for studying spurious molecules in gas mixtures, impressively demonstrated in isotope separation experiments [31–33]. Cluster-specific R2PI, if at all, can only be achieved if there are cluster-specific differences in the excitation spectra. This in general means that the absorption band of the chosen transition should be very narrow, i.e. that inhomogeneous broadening is small. Nowadays most spectroscopic work in this area is done with supersonic beams, where extremely low vibrational and rotational temperatures of the molecules are achieved.

1C-R2PI spectra help us to elucidate the electronic-state energetics of the clusters. A basic advantage of R2PI compared with LIF-spectroscopy is its mass-selectivity which, it should be admitted, may be devaluated in 1C-R2PI by the possibility of photofragmentation. In LIF the absorbing species in the supersonic beam are not easy to identify.

Hopkins et al. [29] published 2C-R2PI spectra of homogeneous benzene clusters which demonstrated the importance of photofragmentation in 1C-R2PI spectra. In cases where the 1C-R2PI spectra show discrete lines, those resulting from photofragmentation of larger clusters can normally be identified by the appearance of the same lines in the spectra of larger parent clusters (if accidental coincidences are excluded by probability). The original excitation spectrum for a specific parent cluster can be measured if its ionization threshold lies below the fragmentation threshold for the larger cluster ions, which is generally expected to be the case. It is clear from this additional condition that cluster-specific excitation spectra which are free from fragmentation features can only be obtained in a 2C-R2PI experiment.

Our 1C-R2PI experiments were therefore undertaken in preparation of future 2C-R2PI experiments. The main objectives were to elucidate the type of excitation spectra one has to be aware of in dealing with clusters and to make sure that each cluster has its own fingerprints in the excited-state energetics by virtue of which it may be selectively ionized.

2. Experimental

A schematic representation of the apparatus for the laser spectroscopy of clusters produced in seeded supersonic beams is presented in fig. 1. We shall now describe in some detail components of our system.

2.1. Apparatus

The beam apparatus consists of a big main chamber (MC) – 155 cm in diameter – which contains two differentially pumped expansion chambers (EC). In both a supersonic beam may be produced, which may be crossed in the MC under

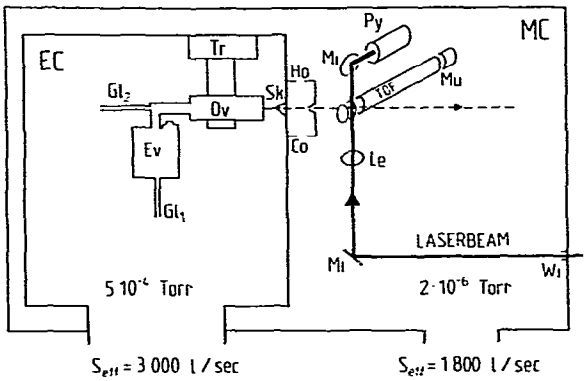

Fig. 1. Schematic representation of the apparatus. EC = expansion chamber, MC = main chamber, Ov = oven (p_0, T_0, d), Tr = translator, Ev = evaporator, Gl = gas line, Sk = skimmer, Co = collimator, Ho = collimator holder, Pr = pressure transducer, TOF = TOF mass spectrometer, Le = lens, Mi = mirror, Py = pyroelectric detector, Mu = particle multiplier, Wi = quartz window.

90°. The detection system is angle selective. All detection components are mounted on an optical bench which is mounted on a big ball-bearing ring (147 cm in diameter). The latter can be driven via a vacuum feed-through by an external stepping motor. In this setup molecular-beam scattering experiments can be performed. For the present experiments only one beam was used. The apparatus is designed so that after an initial optical alignment of the beam sources and the detection system with open MC, no further adjustments are necessary, even for components which are repeatedly removed or replaced. To avoid misalignment of the beam under vacuum caused by walk-off of the bottom of the MC during evacuation both ECs are mounted on a heavy rod system, which is mounted on the stationary part of the ball-bearing ring. Flexible bellows connect each EC to its diffusion pump, mounted on the bottom of the MC.

2.2. *Pumping system*

Continuous beam sources are expected to be best suited for the production of clusters with a repeatable distribution of cluster sizes. Therefore, the beam was designed for continuous mode, making an efficient pumping system necessary. Each EC is evacuated by a 16-inch oil diffusion pump (Varian VHS 400) with a nominal pumping speed of 8000 ℓ/s for air. A water-cooled chevron baffle and a high-vacuum plate valve (Balzers PVA 500 P) reduce the pumping speed to $\approx$ 3000 ℓ/s. Each diffusion pump is backed via a cryotrap by two rotary fore-pumps (Balzers DUO 60 A), each with a pumping speed of 60 m^3/h. The MC is evacuated by two cryopumps with integrated swing valves (Varian VK 12). Their net pumping speed is $\approx$ 1800 ℓ/s. For the present experiment with one beam source the diffusion pump of the second EC was used for additional pumping of the MC especially in experiments with He expansions. The ultimate pressure reached in the MC was some 10^{-8} Torr, whereas the pressure under typical working conditions is 10^{-6} Torr. In the EC the pressure ranges from 10^{-6} to 10^{-3} Torr depending on beam-source parameters.

2.3. *Nozzle source*

Each beam source consists of three parts: (1) A high pressure cell, called oven (Ov), which is mounted on a linear translator (Tr), (2) a skimmer (Sk) and (3) a collimator (Co). Two types of ovens are available, which can be easily exchanged. One can be cooled by pumping a cryogenic fluid through it. The other oven, normally used, can be heated up to 600 K by thermocoax. It is connected with a heatable vessel for the evaporation of fluids (Ev). The nozzle flange of each oven is sealed by an O-ring, which is replaced at higher temperatures by a metal sealing. The nozzle holes are mechanically drilled. Their diameters range from 25 to 150 μ. We normally use a 80 μ nozzle. The pressure in the oven is measured by a differential pressure transducer (Bell and Howell 4-317) which is temperature compensated from 300 to 585 K and which covers a pressure range from 1 to 20 bar. Two thermocouples allow measuring the temperature at the nozzle and the evaporator vessel. The oven is mounted on a linear, dc-driven translator by which the distance d_{NS} between nozzle and skimmer can be varied from 1 to 30 mm. There are two flexible gas lines (GL), one going directly into the oven, the other into the evaporation vessel. If liquids are evaporated and their vapor seeded in a rare-gas diluent, the second gas line is used for the carrier gas to achieve a more uniform mixing of both gases.

Upon expanding into the EC the central portion of the gas jet is skimmed by a 1 mm Campargue type skimmer (SK) [36]. The optimal nozzle–skimmer distance d_{NS} in most experiments was 7 mm. At a distance of 46 mm from the skimmer the beam passes a conical collimator (Co) mounted on a cylindrical holder (Ho). The latter is pumped through large slits from the MC. The interaction region with the laser is ≈ 100 mm down-stream from the nozzle.

For a typical Ar stagnation pressure p_0 of 1.5 bar and a nozzle diameter d of 80 μ the total throughput at the nozzle is ≈ 1 Torr $\ell\ s^{-1}$ corresponding to 3×10^{19} particles s^{-1}. The throughput at the skimmer is reduced by about two orders of magnitude. The following relation has been established for the terminal Mach number of Ar beams: $M_t = 133(p_0 d)^{0.4}$ [2]. This results in a value of $M_t = 23$ for the source parameters mentioned above. In the case of fluorobenzene (FB) seeded in such an Ar beam at a concentration of 2% FB one gets a value of 10^8 particles as a rough estimate for the number of FB molecules contained in the ionization region.

2.4. Seeding technique

When producing free jets with large molecules, with many internal degrees of freedom, only very poor cooling can be achieved [37]. For benzene and some of its substituted derivatives, even at values of $p_0 d = 20$ Torr cm, no clusters could be detected in the beam after mass analysis with an electron-bombardment ionizer and a quadrupole MS.

An efficient method of cooling down these molecules is seeding them in small concentrations into a carrier gas [1,2,37]. Systematic investigation of the R2PI spectra of FB seeded at room temperature (equilibrium vapor pressure 85 Torr) in different carrier gases like CH_4, CO_2, N_2, He, Ar, Kr revealed that the rare gases are most effective for achieving low beam temperatures. Excellent rotational and vibrational relaxation was accomplished with Ar at a moderate value of $p_0 d = 6$ Torr cm. With Kr similar results were found. With He the necessary $p_0 d$ values were about a factor of two higher for comparable relaxation. Similar observations are reported and discussed by Amirav et al. [22]. The relaxation of FB seeded in He and Ar at various stagnation pressures will be discussed more quantitatively in the part of this paper dealing with the spectroscopical results.

2.5. Mass spectrometer

A quadrupole mass spectrometer (Balzers MG 500) combined with an electron impact ionizer was used to analyse the purity of the gases and the total composition of the particle beam produced in the supersonic nozzle source. We preferred however a TOF mass spectrometer (TOF MS) when we ionized the molecules by R2PI with a tunable laser because of its intrinsic advantages. The short duration of the laser pulses ($\tau_p \approx 3$ ns) and the small focusing spot in the ionization region ($D_t \approx 200$ μ) are optimal for an excellent definition of the ion flight times. At the same time a disadvantage of the R2PI method with pulsed lasers can be partially compensated. The low repetition rate of the laser ($\tau_R \approx 50$ Hz) and the short pulse length ($\nu_p \approx 3$ ns) result in a very low duty cycle (10^{-7}). Therefore ideally all ions produced per laser shot should be collected, a demand which is met with a TOF MS. Another often ignored advantage of the TOF MS is that ions which fragment along their flight path are not lost in the spectrum, at least for low initial energies of the fragments. Our home-made spectrometer has a double-field source. Both acceleration regions are 5 mm long. The laser beam intercepts the jet at a right angle in the middle of the first region. The field-free drift space is ≈ 55 cm long. The acceleration voltages are optimized to a first-order spatial focusing according to the theory of Wiley and McLaren [38]. The ions are collected and amplified in a 17 stage Cu/Be-ion multiplier (Balzers SEV 217). To avoid Doppler broadening of the mass peaks and to reduce the deterioration of the transmission by scattering in the poorly pumped flight tube, the axis of the TOF MS is oriented at a right angle to both the molecular and the laser beam. In this configuration the ions have a velocity component orthogonal to the axis of the spectrometer, which is common to all particles due to the beam velocity. Because of this the ions un-

dergo a lateral deflection corresponding to their flight times. Therefore only those ions are detected which lie on the mass scale within a transmission window, the width of which depends on the total acceleration voltage and the beam velocity. In studying ions with larger masses and therefore longer flight times a deflection condensor is installed at the beginning of the field-free region to compensate for the lateral momentum. With different deflection voltages the transmission function may be optimized for different flight times. A voltage ramp may be applied to get uniform transmissionover the whole mass scale. For experiments with Ar we accelerate the ions to a total kinetic energy of 300 eV. For this case the transmission window has a width of 300 amu, while the mass resolution has a value of $m/\Delta m \approx 180$ (fwhm). Decreasing the kinetic energy to 90 eV causes the resolution to increase to $m/\Delta m \approx 330$ (fwhm). A 10% loss in transmission is observed, probably due to the greater influence of stray fields and background scattering. At the same time the width of the transmission window is further reduced. When high resolution is not needed, the ion energy is therefore 300 eV. For room-temperature expansions with He, the beam velocity is $\approx 1.7 \times 10^3$ m/s. For that case the ions are accelerated to 3000 V.

2.6. Laser system

The laser system consists of a 1 MW pulsed nitrogen laser (Lambda Phys M1000) which pumps a dye laser (Lambda Physik FL 2000E) setup in an oscillator–amplifier configuration. The bandwidth of the tunable light, measured with a monitor etalon, is 1 cm^{-1} at a wavelength of 520 nm. It may be narrowed to 0.1 cm^{-1} by the use of an angle-tuned intracavity etalon. The temporal laser pulse width, measured with a fast photodiode and an oscilloscope, was 3.5 ns. To excite FB to the first electronically excited state (S_1), the photons must have a wavelength of $\lambda = 264.4$ nm. Therefore, the output of the dye laser has to be frequency-doubled in an SHG crystal. To increase the conversion efficiency the laser beam is polarized. For the wavelength region from 285 to 259 nm we use a KDP crystal (Lambda Physik FL 31). The second harmonic is phase-matched by angle tuning. The energy per pulse is measured by a pyroelectric probe (Laser Precision RjP 735), which has a wide dynamic range (10^{-7}–1 J) and an excellent spectral flatness (250–16 μm). At $\lambda = 520$ nm, with coumarin 152 as dye, we measure pulse energies after the amplifier stage of 150–250 μJ/pulse corresponding to a peak power of $\approx$ 40–70 kW. For the power and beam quality of our laser the SHG has a conversion efficiency of $\approx 2\%$. The fundamental frequency coming out of the crystal is blocked by a color filter (Schott UG 5). To calibrate the absolute laser wavelength, $\approx 2\%$ of the beam is split off and analysed in a high-resolution grating monochromator (Jobin–Yvon HRS 2). The frequency-doubled light is directed via two mirrors through a quartz window into the apparatus and focused with a 200 mm focal length lens onto the seeded supersonic beam. We measured the diameter D_W of the focusing spot with a sheet of paper and an alignment telescope and got a value of $D_W \approx 200$ μ as an upper limit. Using this value one calculates a peak power density of 4×10^6 W cm^{-2}. The ionization volume defined by the overlap of the laser and the molecular beam is estimated at 10^{-4} cm^{-3}. For such a low power density no fragments appear in the TOF spectrum of FB seeded in Ar. This observation is in accord with the observations reported by Boesl et al. [25,26].

The absolute wavelength is either calibrated with the monochromator or directly from the known frequency for the $S_1 \leftarrow S_0$ origin band of FB. The relative reproducibility of the wavelength is specified by the manufacturer to be 0.05 Å. To normalize the ion current to the laser intensity, the laser beam is directed after the interaction region onto a pyroelectric energy probe placed in the MC.

2.7. Process control, data acquisition and analysis

A schematic block diagram of the setup for the measurement of the R2PI ion yield curves is presented in fig. 2. In the following part we will discuss features concerning process control and signal processing.

The current signal from the multiplier is trans-

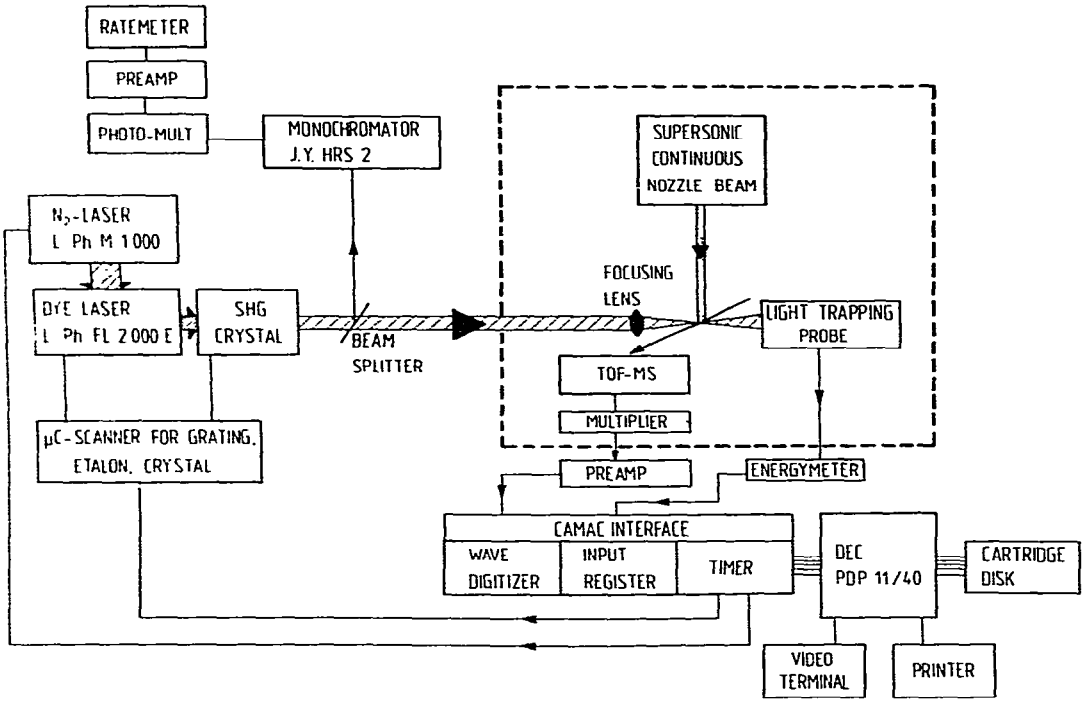

Fig. 2. Block diagram of the experimental arrangement. The MC is symbolized by the block enclosed in broken lines.

formed into a voltage signal which is amplified (10×) in a broad-band preamplifier (PAR 115) and analysed time-correlated to the laser pulse in a high-speed transient digitizer. This analogous detection system is preferred to pulse counting for two reasons. Normally many ions (10–5000) are produced within the peak width ($\tau_W \approx 75$ ns) of a single-ion mass line in the TOF spectrum, each having a pulse width of 5–10 ns. We studied the TOF spectrum for a single laser shot with a very fast storage oscilloscope and observed pulse pileup. For this reason a TDC counting technique is impracticable. For the analogous measurement of ion intensities varying largely with laser wavelength, the linearity of the multiplier amplification is critical. We therefore varied the multiplier voltage to check the influence of saturation. All measurements are made with multiplier voltages U_M where the relative ion intensities are independent of U_M.

The analogous signal processing instrumentation is built up from modular Camac components for reasons of higher flexibility and more efficient on-line control. The Camac crate is connected to a PDP 11/40 minicomputer. The transient digitizer used has a maximal time resolution of 25 ns and a sensitivity of 2 mV per count. It is built up from two 20 MHz waveform digitizers (WD) (Le Croy model 2256A) each with 1024 channels and 8 bit resolution, operated with an external programable clock generator (Le Croy 8501). The clock works in multiphase mode – two 20 MHz clocks, interleaved at 25 ns intervals – leading to an overall time resolution of 40 MHz. The following procedure for measuring a TOF spectrum was established for each sampling cycle. The N_2-laser is externally triggered by a pulse from a programable counter (Borer 1008) which at the same time starts a second counter. This one gives an output pulse after a programable delay, which is used as stop trigger for the freely running WD. After each sampling cycle the content of the WD is transferred to the minicomputer for signal averaging

and further signal processing. To achieve a rapid conversion all Camac programs are written in Macro assembler. The highest transfer rate achieved for the 2048 channels is ≈ 100 Hz. The jitter between the trigger pulse for the N_2-laser and the light pulse is ≈ 2 ns. Every TOF spectrum is integrated over many laser shots (100–500). After a completed run, it may be displayed on a graphic CRT terminal (Lear Siegler ADM 361). A cartridge disk system (DEC RK05) is used for data storage. A hardcopy of the graphics may be made with an alphanumeric/graphic plotter (Anadex DP 9501).

The following procedure was used to measure the wavelength dependence of the R2PI current signal for a certain ion mass. The scanning of the dye laser is controlled by its own microcomputer (Lambda Physik FL 582) which controls up to three different stepper motors (grating, etalon, crystal). For the present experiments the function with automatic crystal/grating tracking is used. A nearly constant output from the SHG crystal is achieved over a scanning range of 150 Å. The communication between the laser system's microcomputer and the PDP 11/40 is established very simply. The sampling interval between two laser scanning steps is controlled by a preset counter which gets its input pulses from the Camac timer. After a complete sampling interval the Camac timer waits a certain programable time interval needed by the laser system to execute the next tuning step. Thereafter the sampling cycle starts anew. For every scan up to eight mass peaks of the TOF spectrum may be integrated over free interval limits. To normalize the ion yield to the laser intensity, the energy per laser shot is measured by a pyroelectric probe and averaged over 100 shots in a microcomputer-based energy meter (Laser Precision Rj 7000). The result is transmitted to the PDP 11/40 via a Camac input register (Borer 1031A). For the normalization we use a variable exponent in the relation describing the dependence of the ion yield on laser power. Its value is empirically determined and varies between 1.5 and 2. This is an indication that for our experimental conditions saturation in the first step is low [26]. We record the variation of the averaged energy per laser pulse for each ion-yield curve.

The laser normally runs at 50 Hz. The sampling time per wavelength interval varies between 2 and 10 s. The typical laser scanwidth for a run is 15 Å with a scanning stepwidth of 0.15 Å.

3. Results and discussion

Fig. 3 shows a TOF spectrum for a mixture of 9% fluorobenzene (FB) in Ar at a total pressure of 1.25 bar, expanded through a 80 μ nozzle and ionized by R2PI. The wavelength of the laser was shifted 1 Å to the red side of the origin band of the first excited singlet state of the monomer (λ_{00} = 2644 Å). For this wavelength the intensity of the FB^+ peak is two orders of magnitude smaller than in the origin band which has a width of 0.27 Å (fwhm) for the cold FB molecules in the beam. The voltages at the TOF MS were tuned for highest resolution. Therefore, only the clusters up to the quadromere could be sampled within the time base of 51.2 μs of our recording system. The TOF peak width (fwhm) was ≈ 75 ns, mainly due to transit time dispersion of our detection system. No chemical fragments could be detected for the low laser power used in the experiment. From that observation we conclude that processes with three or more photons can be neglected.

Fig. 4 portrays a section of the TOF spectrum displayed in a plot, linear in relative mass numbers for a mixture of 2% FB in Ar at a total pressure of

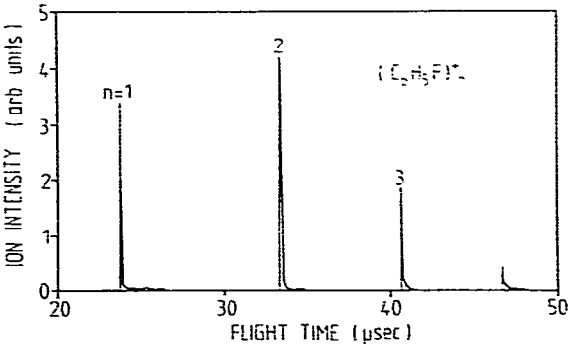

Fig. 3. TOF mass spectrum after R2PI for a mixture of 9% fluorobenzene seeded in Ar at a total pressure of 1.25 bar and expanded through a 80 μ nozzle. The wavelength was shifted 1 Å to the red side of the origin band of the monomer (λ_{00} = 2644 Å).

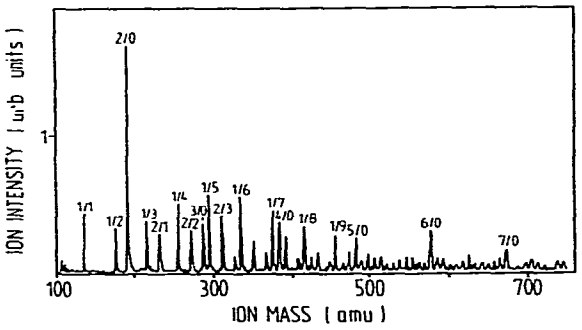

Fig. 4. Mass spectrum for a mixture of 2% FB seeded in He at a total pressure of 5 bar expanded through a 50 μ nozzle at room temperature and analysed after R2PI in a TOF MS. The numbers n/m for each mass peak represent the association numbers of the cluster $FB_n \cdot Ar_m^+$. The laser was tuned 1.6 Å to the red side of $\lambda_{00} = 2644$ nm. The spectrum was integrated over 5000 laser shots.

5 bar, expanded through a 50 μ nozzle at room temperature. The wavelength of the laser was redshifted 1.6 Å relative to λ_{00}. A voltage ramp was applied to the deflection plates of the TOF MS to get a nearly uniform transmission over the whole mass range. In addition to homogeneous clusters FB_n^+ ($n = 1 \ldots 7$) the spectrum shows a lot of heterogeneous clusters $FB_n \cdot R_m^+$ (with $n \leqslant 1 \ldots 7$ and $m \leqslant 1 \ldots 10$) marked in fig. 4 by their association numbers n/m. There is an enhanced underground in the spectrum, probably due to fragmentation of vdW complexes in the acceleration region. As was discussed in the introduction this complexity of the cluster distribution means a drawback in 1C-R2PI due to the possibility of

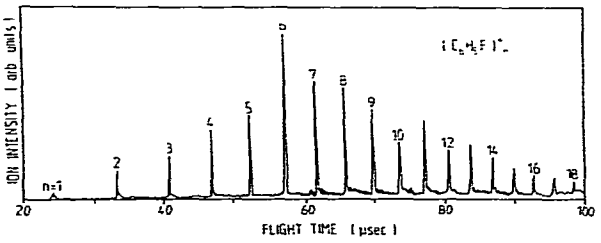

Fig. 5. TOF spectrum for a 2% mixture of FB in Ar at a total pressure of 5 bar and expanded through a 25 μ nozzle. The laser wavelength was shifted 5 Å to the red of the monomer origin.

photofragmentation. No such heterogeneous clusters were found for expansions of FB in He. Therefore we preferred He as carrier gas for the spectroscopy of the homogeneous clusters. Fig. 5 shows a TOF-spectrum for a 7% mixture of FB in Ar at a total pressure of 5 bar and expanded through a 25 μ nozzle. The laser wavelength was shifted 5 Å to the red of λ_{00}. A voltage ramp was applied at the condensor of the TOF MS. The spectrum shows homogeneous clusters for up to FB_{19}^+, with a maximum at FB_6^+. All these cluster spectra clearly do not reflect the cluster-size distribution in the neutral beam. For a fixed laser wavelength every cluster shows a different absorption coefficient in the excitation step and a different and yet unknown fragmentation pattern upon ionization. The maximum in the TOF spectrum generally shifts to higher mass numbers with increasing laser wavelength due to an increased redshift of the absorption maximum of the clusters with increasing aggregation number.

What can we learn from these mass spectra? On the one hand, they demonstrate the complexity of the cluster-size distribution in the beam at even medium-expansion conditions especially for expansions with Ar. On the other hand, they demonstrate the sensitivity and mass resolution of the detection system. Meaningful spectroscopic information for clusters produced in seeded supersonic beams can only be obtained by careful selection of the source parameters and the carrier gas in conjunction with mass analysis.

3.1. Temperature-cooling effect in the seeded beam

To get an idea of the temperature in the supersonic beam we first studied the FB^+ signal as a function of the laser wavelength in the 2644 Å region. Because of the resonant excitation step of R2PI we should get a spectrum corresponding to the 0–0 and to vibronic excitations of the $S_1 \leftarrow S_0$ ($^1B_2 \leftarrow {}^1A_1$) electronic transition of the FB monomer. The relevant level diagram is portrayed in fig. 6. Fig. 7a shows the R2PI spectrum for a 20% mixture of FB in He at a total pressure of 0.2 bar and expanded through a 80 μ nozzle at room temperature. The dominant feature is the origin band (ν_{00}) at 37816 cm^{-1}. A hot-band system

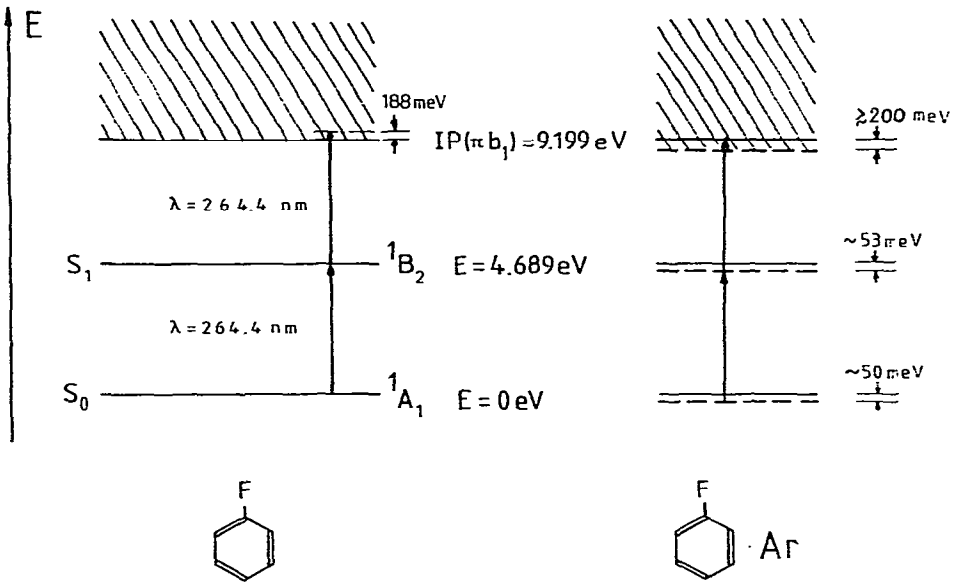

Fig. 6. Level diagram for 1C-R2PI of fluorobenzene. The estimated energy levels for FB·Ar at equilibrium distance are shown by broken lines for comparison.

extends to its low-frequency side. The positions of these bands relative to ν_{00} are given in table 1 and compared with the data of Lipp et al. [39–41]. The agreement between their vapor-phase absorption spectrum and our results from the R2PI spectrum is very good. We found additional weak bands and reproduced them in measurements with different mixtures of FB in He at different total pressures. Based on the analysis of Lipp et al. a tentative assignment for these previously not recorded bands is proposed, also given in table 1. The relative intensities of the hot-bands in the R2PI spectrum are substantially lower than those of the absorption spectrum, indicating considerable vibrational and rotational relaxation for the molecules in the low-pressure He expansion. From the vibrational frequencies in the literature [39–41] one evaluates for the spectrum in fig. 7a a different vibrational temperature T_{vib} for the different hot-bands, providing evidence for a non-Boltzmann vibrational distribution in the jet. The higher the frequency of the vibrational mode, the higher the vibrational temperature. For the 11_1^1 hot-band at -65 cm^{-1} in fig. 7a, one evaluates $T_{vib} \approx 140$ K, using a ground-state fundamental of 248.6 cm^{-1}. For the $18b_1^1$ band at -17 cm^{-1} with a fundamental of 403.6 cm^{-1} the value is $T_{vib} \approx 230$ K. This non-Boltzmann character of the vibrational distribution in molecules relaxated in supersonic expansions was also reported by Murakami et al. [42]. It may justify the proposed assignments for the weak hot-bands in cases, where even for the unrelaxed high-frequency modes low intensities are calculated. Fig. 7b shows a part of the spectrum of fig. 7a for a 0.3% mixture of FB seeded in He at a total pressure of 4.4 bar and expanded through a 80 μ room-temperature nozzle. In addition to the origin band, whose width is further reduced to 4.5 cm^{-1}, the $18b_1^1$ band appears with an intensity of 3% and the 11_1^1 and $6a_1^1$ bands with intensities of $\approx 1\%$ relative to that of the origin band. One evaluates for the 11_1^1 band $T_{vib} \approx 75$ K and for the $6a_1^1$ band $T_{vib} \approx 160$ K. As for the rotational temperature in the beam one may assume that it is close to the translational temperature, T_{trans}, of the carrier gas, which is evaluated at ≈ 3–5 K under typical expansion conditions.

These observations led us to the following ad-

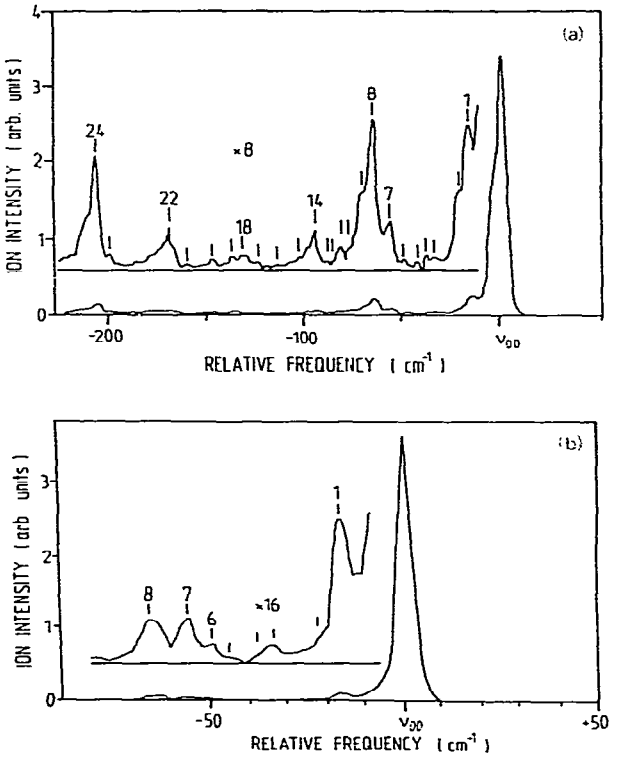

Fig.7. Ion current versus photon energy (cm^{-1}) for FB^- in the region of the 0–0 transition at $\nu_{00} = 37816\ cm^{-1}$. The assignment of the hot-band system is listed in table 1. (a) The expansion consisted of a 20% mixture of FB seeded in He at a total pressure of 0.2 bar and expanded through a 80 μ room-temperature nozzle. (b) Part of the spectrum in (a) for a 0.3% mixture of FB in He at a total pressure of 4.4 bar, the other source parameters were the same as in (a). Both spectra were averaged over 100 laser shots. The multiplier voltage was 2 kV.

Table 1
Band positions and assignments of the hot-band system of the S_1 state of fluorobenzene in the 2644 Å region

Number	$\Delta\nu = \nu_{00} - \nu$ [a] (cm^{-1})	$\Delta\nu = \nu_{00} - \nu$ [b] (cm^{-1})	Assignment [c]
1	17.1	16.9	$18b_1^1$
2	22	24.8	?
3	33.8	(32.9)	$18b_2^2$)
4	38.1	(40.5)	(1_1^1?)
5	44.4	(45.0)	(12_1^1)
6	49.9	50.4	($18b_2^3$?)
7	57.1	57.4	$6a_1^1$
8	65.9	65.8	11_1^1
9	72.4	(73.4)	($18b_2^2 1_1^1$?)
10	77.5	(75.2)	
11	81.9	82.6	$11_1^1 18b_1^1$
12	85.4	(85.6)	($1_1^1 12_1^1$)
13	89.9	(90.0)	($12_2^1 15_1^1$)
14	95.2	95	$6b_1^1$
15	102.8	(102.4)	($12_1^1 6a_1^1$)
16	114.2	(114.8)	($6a_2^2$)
17	124.4	124.9	$6a_1^1 11_1^1$)
18	132.4	131.9)	11_2^2
19	138.2	(140.6)	($12_1^1 6b_1^1$)
20	147.7	148.1	$11_2^2 18b_1^1$
21	161.0	160.0	$11_1^1 6b_1^1$
22	168.9	168.6	$16b_1^1$
23	200	200	$10b_1^1$
24	206.2	206.0	$16a_1^1$

[a] The estimated accuracy of the frequencies relative to the electronic origin is $\pm 1.5\ cm^{-1}$.

[b] The band positions are from Lipp et al. [39–41]. Those in parentheses are calculated with the constants from the same publication according to the proposed assignment in the fourth column.

[c] The assignments were taken from Lipp et al. [39–41] with exception of those in parentheses which are proposed for the first time.

vantages of R2PI spectroscopy in combination with supersonic beams. The analysis of the spectra may be simplified by studying their dependence on the expansion parameters. By variation of the gas-dynamic cooling of the molecules hot-bands can be easily distinguished in the spectrum. Bands buried on conjested sequences are easier detected and investigated due to a substantial narrowing of the rotational envelopes. Spectral features from clusters may be similarly identified. The detection efficiency in most cases is very high.

3.2. Spectra of heterogeneous clusters

Seeding FB in Ar leads to an efficient cooling of the beam at even lower stagnation pressures than with He. Similar results were reported by Amirav at al. [22]. Fig. 8a shows the intensity of the FB^+-ion yield versus the energy of the photons for a 2.5% mixture of FB seeded in Ar at a total pressure of 1 bar and expanded through a 80 μ nozzle. The wavelength was scanned between 264 and 265 nm. The scan width was 0.009 nm. The

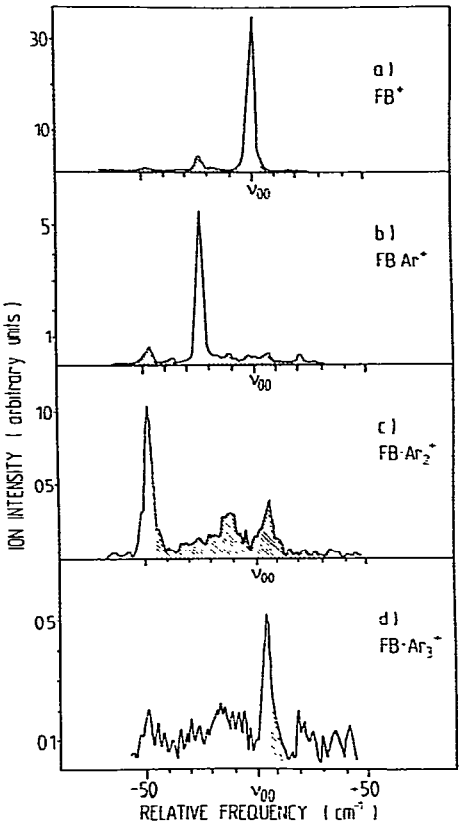

Fig. 8. Ion-yield curves of various molecules versus the photon energy (cm^{-1}) for a 2.5% mixture of FB seeded in Ar at a total pressure of 1 bar and expanded through a 80 μ room-temperature nozzle. The ions detected are: (a) FB^+, (b) $FB{\cdot}Ar^+$, (c) $FB{\cdot}Ar_2^+$, (d) $FB{\cdot}Ar_3^+$. The spectral features assigned to photofragmentation of higher clusters are hatched. All spectra were measured simultaneously during one run. Each data point is the average over 400 laser shots. The scanning range of the laser was ± 150 cm^{-1} relative to ν_{00}. Only the part of the spectra, which shows prominent structure, is shown.

ion intensity was normalized to the square of the laser power. Each data point represents the intensity integrated over 400 laser shots. Beside the 0–0 band no vibrational hot bands with intensities greater than 1% are observed. But in contrast to fig. 7b two satellite bands appear at -46 and -23 cm^{-1}, relative to ν_{00}. These spectral features only appear for expansions with Ar. They are due to the ionization of heterogeneous vdW clusters $FB{\cdot}Ar_n$ ($n = 1, 2$) which photofragment to FB^+. These satellite bands slightly displaced from the electronic transition of the uncomplexed molecule were observed for a number of molecules with associated rare gas atoms as has been discussed by Levy [1,2]. Figs. 8b–8d show the wavelength dependence for the production of the ions $FB{\cdot}Ar^+$, $FB{\cdot}Ar_2^+$ and $FB{\cdot}Ar_3^+$ measured in the same run as that of FB^+ shown in fig. 8a. Following prominent spectral features can be observed: All spectra for these complexes show only one dominant band. Their shifts relative to ν_{00} are given in table 2. This observation provides evidence that for these complexes only one chemically stable isomer exists.

The shifts of the origin band from FB to $FB{\cdot}Ar_2$ are strictly additive with -23 cm^{-1} for each Ar associate. This is not the case for $FB{\cdot}Ar_3$, which shows a shift of 4.8 cm^{-1}. Levy et al. [1,2] have observed that for the iodine complexes I_2R_n (R = rare gas) the spectral shift is a linear function of n (for R = Ne up to $n = 6$). They formulated a band-shift rule for these complexes which postulates additivity in the shift per added rare-gas atom. The physical basis for their observation is not well understood [1,2]. Evidence is currently growing that this rule is only approximately valid for complexes of aromates with rare gases [1,2,43]. The exact additivity of the shifts for FBAr and

Table 2
Spectral shifts of the electronic origin of the S_1 state of fluorobenzene·R_n complexes from the electronic origin ν_{00} of the bare molecule, together with the probability of the complexes to fragment upon ionization into different channels by unimolecular decay

Species	$\Delta\nu = \nu_{vdW} - \nu_{00}$ [a,b] (cm^{-1})	Probability of fragmenting upon ionization to	
		FB^+	$FB{\cdot}R^+$
FB·Ar	−23 (43) +20	43%	
$FB{\cdot}Ar_2$	−46	35%	26%
$FB{\cdot}Ar_3$	+4.8		
FB·Kr	−37 (41.6) +4.6	60%	
$FB{\cdot}Kr_2$	−74		

[a] Accuracy of the spectral shifts is ± 1.5 cm^{-1}.
[b] The values in parentheses are the difference of the shifts for the bands of a doublet, assigned to the frequency of a vdW mode.

$FBAr_2$ may be explained by the assumption that the Ar atoms in both complexes occupy geometrical equivalent sites on the axis vertical to the ring plane. The distance from the ring center should be similar to that found for benzene · Ar complexes [27], namely 3.4 Å. These arguments are not valid for $FB \cdot Ar_3$. Each shift carries information about the vdW potentials of both the ground and the first electronically-excited singlet state of the molecule and can be expressed by $\Delta\nu = \nu_{vdW} - \nu_{00} = D_0'' - D_0'$. It is therefore a measure for the differences between the zero-point vdW dissociation energies D_0 of the two states. The shift is always small, probably amounting to not more than 20% of the binding energy [1,2]. A red-shift indicates that the excited-state potential is deeper than that of the ground state. Fig. 6 also shows a rough energy-level diagram for FB · Ar. The hatched bands in figs. 8a–8d are due to photofragmentation of the vdW complexes. Before we go into details, a short comment should be made on this fragmentation channel. As can be seen on the energy level diagram of fig. 6, the energies of two photons at 2644 Å add up to 9.378 eV, corresponding to an excess energy of 188 meV (1516 cm^{-1}) above the ionization limit. Depending on the Franck–Condon factors (FC) of the transition, this energy either can be taken off as translational energy by the electron or can be converted into internal vibrational excitation of the ion. In the ionization of the FB monomer with one photon, $\Delta\nu = 0$ transitions are strongly favored due to the fact that the geometry of the ion is nearly the same as that of the neutral molecule. Photoionization of cold monomer molecules therefore produces vibrationally cold ions which cannot fragment [29]. A recent study [44] of the photoelectron spectra from R2PI of toluene clearly demonstrates the validity of the same propensity rule for $\Delta\nu = 0$ transitions for the two-step ionization process. As has already been pointed out by Hopkins et al. [29], these arguments are not applicable to the case of vdW complexes. The neutral clusters are bound by means of weak electrostatic polarization interaction, in the case of FB · Ar with a binding energy of roughly 50 meV (400 cm^{-1}) [28], the $FB \cdot Ar^+$ cluster, on the other hand, is bound much more strongly by monopole-induced dipol interaction. In this case the FC factors favor large changes in the vibrational quanta of the intermolecular vibration modes and a large fraction of the excess energy can end up in vibrational degrees of freedom of the complex ion. The unexpected small red shift in the ionization potential for the benzene · Ar cluster of 21.2 meV relative to that of the pure benzene molecule reported by Fung et al. [28] may be understood by the same arguments. The vibrationally hot vdW molecules therefore may fragment by predissociation if their vibrational energy is larger than D_0^+, the dissociation energy of the complex ion.

In the spectrum of FB^+ (fig. 8a) the hatched bands assigned to photofragmentation have their counterparts in the major resonances of the spectra for $FB \cdot Ar_n^+$ ($n = 1 \ldots 3$) (figs. 8b–8d). Taking the spectrum of $FB \cdot Ar^+$, the band at -46 cm^{-1} coincides with the origin band of $FB \cdot Ar_2^+$. The spectral features at -11 and $+6$ cm^{-1} appear equally in fig. 8c. For a higher pressure (fig. 9b) they are strongly enhanced and may therefore be attributed to parent clusters $FB \cdot Ar_n$ ($n > 3$). At low Ar pressure the band at -36 cm^{-1} appears neither in the spectra of $FB \cdot Ar_2^+$ nor of $FB \cdot Ar_3^+$, but is probably also from a parent molecule with more than three Ar associates. The blue-shifted band at 19.6 cm^{-1} can definitely be assigned to the FB · Ar complex. It is also listed in table 2. From this analysis a doublet structure for FB · Ar is deduced which can hardly be explained by the existence of two different isomers. We therefore assign the 19.6 cm^{-1} band to the excitation of a vdW stretching mode of the Ar atom with respect to the ring plane. The vibration frequency from that assignment is 43.4 cm^{-1} which is reasonable for an aromat · Ar complex [45]. It should be noted that, in addition to the origin band, Leutwyler et al. [45] observed a second band for the fluorene · R vdW molecules, whose shift (relative to the origin of the complex) is 41 cm^{-1} for R = Ar and 63 cm^{-1} for R = Kr. Their interpretation is similar to ours although they could not strictly exclude the existence of isomers. As for the spectrum of $FB \cdot Ar_2^+$ (fig. 8c) the two bands at -10.7 and $+6.3$ cm^{-1} are presumably also from photofragmentation of higher clusters due to a strong intensity increase at higher pressure. In fig. 8d, which shows

the R2PI spectrum of $FBAr_3$ the shoulder at the high-frequency side of the origin band also shows a contribution from the 6.3 cm^{-1} band also seen in fig. 8c. Nevertheless, the band can hardly be explained solely by photofragmentation of higher-order clusters for mainly two reasons. The spectrum was measured for an Ar pressure where higher-order clusters showed only extremely weak intensity in the TOF-mass spectrum. The broad structure, attributed to photofragmentation, gets prominent only for higher Ar pressure (fig. 9d).

From the relative intensities of the fragmentation bands in fig. 8a compared with those for the parent ions in figs. 8b–8d we may estimate the probability for each vdW complex to photofragment to FB^+. The values are summarized in the fourth column of table 2. Because we worked with a constant deflection field at the TOF MS, which was optimized for the $FB \cdot Ar^+$ ions, the exact values may be 5–10% higher. The FB · Ar molecule with excited vdW mode seems easier to fragment than an unexcited one. Figs. 9a–9d show the spectra one obtains after increasing the Ar pressure to 1.7 bar while retaining the other source parameter. The spectral features, assigned to fragmenting higher vdW cluster, hatched in figs. 8a–8d are now strongly enhanced. We also studied the spectra for $FB \cdot Ar_4^+$ and $FB \cdot Ar_5^+$ (figs. 10a and 10b). But at argon pressures, where we observed these clusters with reasonable intensity, all spectra became broader and more complex and the spectral features due to photofragmentation are not easy to identify. Only a two-color experiment may make it possible to unveil the spectra for the higher $FB \cdot Ar_n$ complexes.

Table 2 also contains the shifts we measured for vdW complexes with krypton. Again, strict additivity of the spectral shift is observed as long as

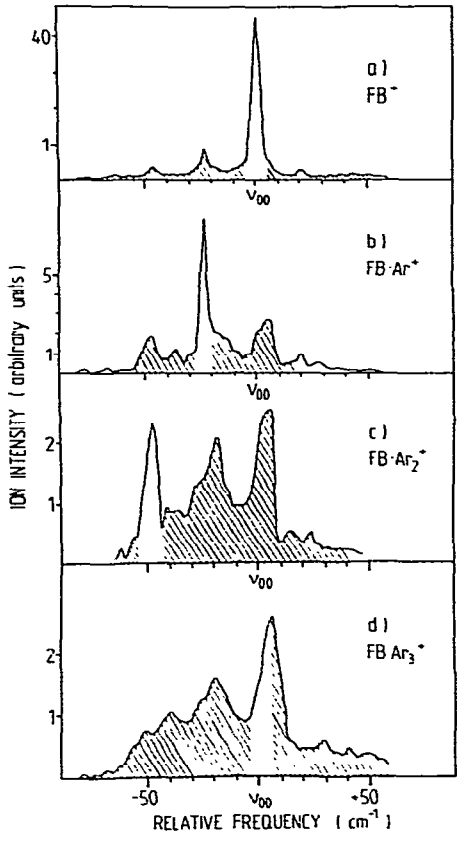

Fig. 9. Ion-yield curves as in fig. 8 but with the total pressure of the expansion increased to 1.7 bar. The ions detected are: (a) FB^+, (b) $FB \cdot Ar^+$, (c) $FB \cdot Ar_2^+$, (d) $FB \cdot Ar_3^+$. The number of laser shots per sampling interval was 100.

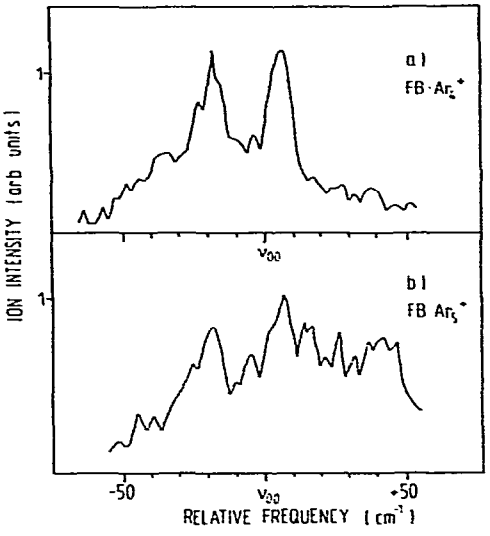

Fig. 10. Ion-yield curves of (a) $FB \cdot Ar_4^+$ and (b) $FB \cdot Ar_5^+$ for a 0.8% mixture of FB seeded in Ar at a total pressure of 3.2 bar and expanded through a 25 μ nozzle at room temperature. The spectral features due to photofragmentation can no longer be unambiguously identified.

only two atoms are added, the shift constant being $-37\ cm^{-1}$. This increase in the red shift is due to a larger polarizability of Kr compared with Ar. A second weak band for FB · Kr at 4.6 cm^{-1} is probably due to an excited vdW mode with a frequency of 41.7 cm^{-1}. Leutwyler et al. found a larger shift of the origin for the fluorene · Kr complexes of $-63\ cm^{-1}$, with a doublet splitting of 30 cm^{-1}.

3.3. Spectra of homogeneous clusters

The R2PI spectra for the homogeneous clusters are basically more complex than for the heterogeneous clusters just presented. The intensity of FB_2^+ versus laser wavelength for various expansions of FB seeded in He is shown in figs. 11a–11c. Instead of a simple line spectrum we observed a complex spectrum $\approx 350\ cm^{-1}$ wide, with a double-hump structure. One part is blue-shifted relative to λ_{00}, the maximum of its envelope lying at $\approx 37840\ cm^{-1}$, the other part is red-shifted with the maximum at 37750 cm^{-1}. The blue-shifted part shows more than 12 narrow bands. By cooling the nozzle and diluting the FB/He mixture further to achieve lower temperatures in the beam, the blue-shifted part disappears, as can be seen in fig. 11c.

The broadening of the spectral features for the $S_1 \leftarrow S_0$ transition of the dimer complexes can originate from the following causes:

(1) Nearly isoenergetic conformers may exist, which are produced in the beam in different ratios depending on the expansion conditions. The structure of the FB-dimer in the gas phase is still unknown. That of solid-state fluorobenzene is well known [46]. The crystal belongs to the dihedral space group $D_4^4 = P_{4_12_12}$ or $D_4^8 = P_{4_32_12}$. No direct analogies concerning the structure of the gas-phase clusters can be drawn from these crystal data. Three different conformations are plausible:

(a) A sandwich-type parallel plane conformation, the distance between the planes being roughly 3.5 Å postulated for the benzene · hexafluorobenzene complex [8].

(b) A T-shaped structure analogous to that, postulated for the benzene dimer [47], with the ring centers being roughly 5 Å apart.

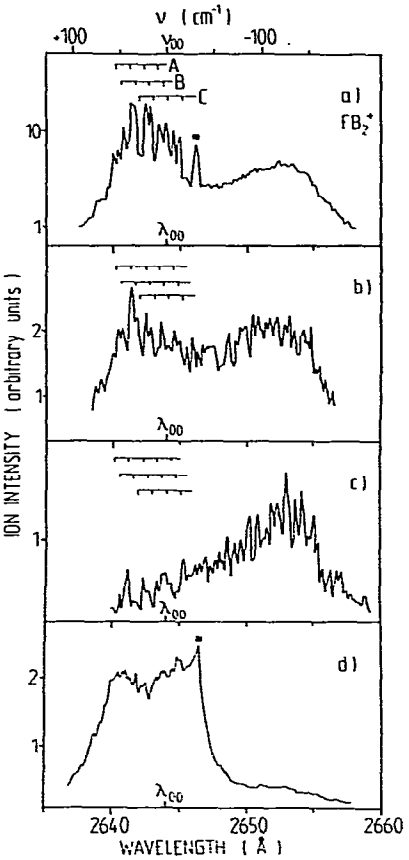

Fig. 11. Ion current of FB_2^+ versus laser wavelength at various expansion conditions. The parameters listed in order: mixing ratio in % of FB in R, nozzle temperature, nozzle diameter, total expansion pressure, and carrier gas R, were the following: (a) 0.07%, 300 K, 80 μ, 4 bar, He. (b) 0.03%, 250 K, 80 μ, 4.2 bar, He. (c) 0.04%, 300 K, 80 μ, 3.5 bar, He. (d) 2.7%, 300 K, 80 μ, 4 bar, Ar. Each spectrum is displayed on a different relative intensity scale. In most cases the spectra were averaged over 100 laser shots.

(c) An in-plane configuration with collinear symmetry axis. Only model calculations or high resolution RF or optical spectroscopy may give an answer to the question of the energetics and structure of these different possible conformers.

(2) Photofragmentation from higher clusters may certainly not be neglected in 1C-R2PI, as has already been discussed for the case of the FB · Ar complexes. From some similarities between the spectrum for FB_3^+ and the blue-shifted part of

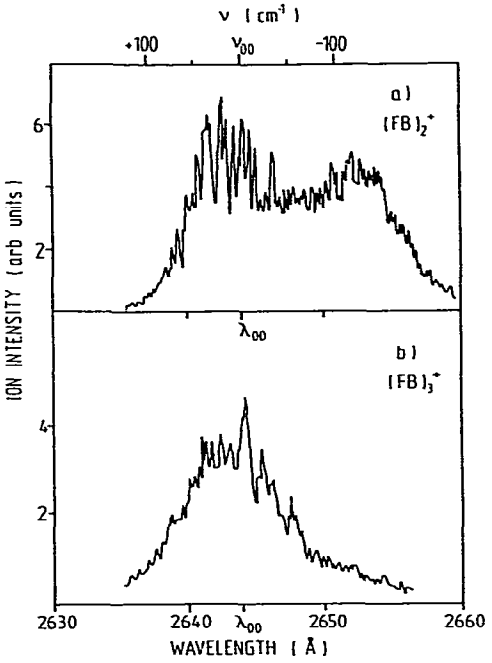

Fig. 12. Ion current versus laser wavelength of (a) FB_2^+, (b) FB_3^+ for a 0.4% mixture of FB seeded in He at a total pressure of 3.12 bar and expanded through a 80 μ room-temperature nozzle. Each data point was averaged over 100 laser shots. The stepwidth of the scan was 0.09 Å.

FB_2^+ (see figs. 12a and 12b) we cannot exclude the possibility that photofragmentation contributes to the spectral features of the dimer spectrum. But it certainly does not explain the characteristic multiline structure in the blue-shifted part of the spectrum which can be observed even with very diluted mixtures where the formation of trimers is strongly suppressed. With regard to the red-shifted part of the dimer absorption shown in figs. 11a–11d, a larger overlap with the absorption spectra of bigger clusters $(FB)_n$ (with $n > 5$) could be inferred from our measurements, so that a contribution from photofragmentation may explain the lack of prominent structure in the spectra for the FB/He mixtures with moderate dilution (fig. 11a). For mixing ratios smaller than 0.03%, this contribution should be drastically reduced due to the low-number density of bigger clusters in the beam.

(3) Vibrational structure due to the excitation of intermolecular motion in the electronically excited state S_1 may appear in the spectrum even if the clusters are vibrationless in the ground-state S_0. A vibrational progression then appears, according to the Franck–Condon factors.

(4) Thermal population of intermolecular vibrational states in S_0 may lead to a superposition of progressions. Due to the masses and the weak vdW interaction of the molecules the frequencies of the vdW modes are expected to be 10–50 cm^{-1}. For such low frequencies the vibrational relaxation is not perfect, even at high p_0d-values. One evaluates for a vdW mode with 10 cm^{-1} and a vibrational temperature of 20 K that only ≈ 50% of the dimers are populating the zero-point vibration while the rest is distributed over vibrationally excited states. Because of their low frequency the intermolecular vdW modes are certainly better relaxed than the intramolecular modes, but it should be taken into account that condensation takes place in a late stage of the expansion and that therefore even at high mass throughput a small amount of condensation energy may survive as intermolecular motion of the complexes.

On the basis of these different cases possibly leading to the spectral complexity of the $S_1 \leftarrow S_0$ transition of the dimer we present a tentative assignment for the prominent features of the FB_2^+ spectrum. The main lines of the blue-shifted part of the spectrum exhibit a structure which may be interpreted as three progressions of 15 cm^{-1}, shifted by 5 cm^{-1}, as shown in figs. 11a–11d. We assign the 15 cm^{-1} to the vdW vibration of the dimer in the S_1 state. The progression B is red-shifted and lower in intensity relative to progression A and shows a decrease in intensity for lower beam temperatures. Progression C is buried in the minima between progression A and B. We assign progression B and C respectively to transitions from an excited vdW state in S_0, which differs by one and two quanta respectively from the state from which progression A starts. With this assignment the vibration frequency of the vdW ground state S_0 must be 20 cm^{-1}, which is larger than the 15 cm^{-1} for the S_1 state. From this difference we may deduce a slightly stronger intermolecular interaction for the dimer in the S_0 compared with the S_1 state. This analysis is also supported by the blue-shift of the lines relative to λ_{00}. It should be

mentioned that from the absorption spectrum of the FB crystal measured at 4.5 K in the same spectral region, the frequency of the lowest lattice vibration was determined to be 16 cm^{-1} [48]. As for the red-shifted part in the spectrum this is probably due to a different conformational isomer. For high total pressures and very dilute FB/He mixtures in the expansion the blue-shifted band system nearly completely disappears while the red-shifted shows a complicated structure (fig. 11c). With Ar as carrier gas the FB_2^+ spectra appear similar to those with He, with the exception that for higher p_0d-values ($p_0d > 24$ Torr cm) the red-shifted hump in the spectrum is substantially suppressed (fig. 11d). The blue-shifted part of the spectrum shows only poor structure. From the observation that the spectra for the FB dimer with and without Ar associates looks very similar, we ascribe the loss of prominent structure in the spectra measured with Ar expansions to an enhanced contribution of photofragmentation from the vdW complexes $FB_2 \cdot Ar_n$. The different dependence of red- und blue-shifted spectral features from beam temperature and carrier gas provides evidence for the existence of different conformational isomers in the beam. It should be admitted, that neither the prominent peak in fig. 11a (marked by an asterisk), nor that in fig. 11d could be explained by this assignment.

Fig. 12b shows the R2PI spectrum of FB_3^+. For comparison purposes, the spectrum for FB_2^+, measured in the same run, is shown in fig. 12a. The absorption spectrum resembles the blue-shifted part of the dimer spectrum in width and position except for four new, prominent bands at -2.6, -20, -29, -50 cm^{-1} relative to ν_{00}. We ascribe these spectral features to the absorption of the trimer but currently have no conclusive assignment.

4. Conclusion

One objective of the study was to investigate the feasibility of cluster-selective R2PI taking advantage of cluster-specific shifts in the excitation step of this two-photon ionization. From the results presented here for fluorobenzene seeded in a rare-gas diluent we provided evidence for the importance of photofragmentation in 1C-R2PI. For the case of $FB \cdot Ar_n$-complexes we observed specific shifts for clusters with different coordination number n, which were additive for up to $n = 2$. In a two-color experiment cluster selectivity should be easy to establish for these heterogeneous complexes. The situation is not as favorable in the case of homogeneous clusters, due to an enhanced spectral complexity. As long as photofragmentation is not strongly reduced in a 2C-R2PI experiment, an unambiguous analysis of the bands is difficult and often even impossible. A further reduction of spectral complexity should be possible with a still better cooling of the beam and an improved exciting laser resolution. With careful optimization of the beam source parameters and proper selection of the excitation transition, cluster-specific ionization spectroscopy seems to be feasible. Experiments with 2C-R2PI are currently being prepared in our laboratory.

Acknowledgement

We gratefully acknowledge the financial support of the Bundesministerium für Forschung und Technologie. Moreover, we thank Dr. Ding and Dr. Illenberger for loans of optical components and Dr. Weigmann for his help in developing part of the computer software.

References

[1] D.H. Levy, in: Advances in Chemical Physics, Vol. 47, Photoselective chemistry, Part 1, eds. J. Jortner, R.D. Levine and S.A. Rice (Wiley–Interscience, New York, 1981) p. 323.
[2] D.H. Levy, Ann. Rev. Phys. Chem. 31 (1980) 197.
[3] J.A. Beswick and J. Jortner, in: Advances in Chemical Physics, Vol. 47, Photoselective chemistry, Part 1, eds. J. Jortner, R.D. Levine and S.A. Rice (Wiley–Interscience, New York, 1981) p. 363.
[4] F.F. Abraham, Homogeneous nucleation theory (Academic Press, New York, 1974).
[5] J.C. Slater and K.H. Johnson, Phys. Today 27, (1974) 34.
[6] T.E. Gough, R.E. Miller and G. Scoles, J. Chem. Phys. 69 (1978) 1588.
[7] M.F. Vernon, D.J. Krajnovich, H.S. Kwok, J.M. Lisy, Y.R. Shen and Y.T. Lee, J. Chem. Phys. 77 (1982) 47.

[8] J.M. Steed, T.A. Dixon and W. Klemperer, J. Chem. Phys. 70 (1979) 4940.
[9] W. Klemperer, Ber. Bunsenges. Physik. Chem. 78 (1974) 128.
[10] J. Erickson and C.Y. Ng, J. Chem. Phys. 75 (1981) 1650.
[11] C.Y. Ng, D.J. Trevor, P.W. Tiedemann, S.T. Ceyer, P.L. Kronebusch, B.H. Mahan and Y.T. Lee, J. Chem. Phys. 67 (1977) 4235.
[12] C.Y. Ng, P.W. Tiedemann, B.H. Mahan and Y.T. Lee, J. Chem. Phys. 66 (1977) 3985.
[13] C.Y. Ng, P.W. Tiedemann, B.H. Mahan and Y.T. Lee, J. Chem. Phys. 66 (1977) 5737.
[14] S.H. Linn and C.Y. Ng, J. Chem. Phys. 75 (1981) 4921.
[15] P.M. Dehmer and S.T. Pratt, J. Chem. Phys. 76 (1982) 843.
[16] E.D. Poliakoff, P.M. Dehmer, J.L. Dehmer and R. Stockbauer, J. Chem. Phys. 75 (1981) 1568.
[17] P.M. Dehmer and J.L. Dehmer, J. Chem. Phys. 69 (1978) 125.
[18] R.E. Smalley, D.H. Levy and L. Wharton, J. Chem. Phys. 64 (1976) 3266.
[19] R.E. Smalley, L. Wharton and D.H. Levy, J. Chem. Phys. 66 (1977) 2750.
[20] R.E. Smalley, L. Wharton, D.H. Levy and D.H. Chandler, J. Chem. Phys. 68 (1978) 2487.
[21] S.M. Beck, M.G. Livermann, D.L. Monts and R.E. Smalley, J. Chem. Phys. 70 (1979) 232.
[22] A. Amirav, U. Even and J. Jortner, J. Chem. Phys. 71 (1979) 2319; 75 (1981) 3770.
[23] T.R. Hays, W. Henke, H.L. Selzle and E.W. Schlag, Chem. Phys. Letters 77 (1981) 19.
[24] S.V. Andreyev, V.S. Antonov, J.N. Knyazev and V.S. Letokhov, Chem. Phys. Letters 45 (1977) 166.
[25] U. Boesl, H.J. Neusser and E.W. Schlag, Z. Naturforsch. 33a (1978) 1546.
[26] U. Boesl, H.J. Neusser and E.W. Schlag, Chem. Phys. 55 (1981) 193.
[27] K.H. Fung, H.L. Selzle and E.W. Schlag, Z. Naturforsch. 36a (1981) 1338.
[[28] K.H. Fung, W.E. Henke, T.R. Hays, H.L. Selzle and E.W. Schlag, J. Phys. Chem. 85 (1981) 3560.
[29] J.B. Hopkins, D.E. Powers and R.E. Smalley, J. Phys. Chem. 85 (1981) 3739.
[30] M.A. Duncan, T.G. Dietz and R.E. Smalley, J. Chem. Phys. 75 (1981) 2118.
[31] H.J. Neusser, Ber. Bunsenges. Physik. Chem. 85 (1981) 168.
[32] S. Leutwyler and U. Even, Chem. Phys. Letters 81 (1981) 578.
[33] O. Dimopoulou, Diplomarbeit FU Berlin, West Germany (1982).
[34] A. Herrmann, M. Hofmann, S. Leutwyler, E. Schumacher and L. Wöste, Chem. Phys. Letters 62 (1979) 216.
[35] B. Brutschy, Attersee-workshop, September 1981.
[36] R. Campargue and A. Lebehot, 9th International Symposium on Rarefied Gas Dynamics, eds. M. Becker and M. Fiebig (Göttingen, 1974) p. C11.
[37] J.B. Anderson, in: Gasdynamics Series, ed. P. Wegener, Molecular beams and low density gasdynamics (Dekker, New York, 1974).
[38] W.C. Wiley and I.H. McLaren, Rev. Sci. Instr. 26 (1955) 1150.
[39] E.D. Lipp and C.J. Seliskar, J. Mol. Spectry. 87 (1981) 255.
[40] E.D. Lipp and C.J. Seliskar, J. Mol. Spectry. 87 (1981) 242.
[41] C.J. Seliskar and E.D. Lipp, Chem. Phys. Letters 59 (1978) 47.
[42] J. Murakami, K. Kaya and M. Ito, J. Chem. Phys. 72 (1980) 3263.
[43] M.J. Ondrechen, Z. Berkowitch-Yellin and J. Jortner, J. Am. Chem. Soc. 103 (1981) 6586.
[44] J.T. Meek, S.R. Long and J.P. Reilly, J. Phys. Chem. 86 (1982) 2809.
[45] S. Leutwyler, U. Even and J. Jortner, Chem. Phys. Letters 86 (1982) 439.
[46] D.E. Henshaw, Acta Cryst. 14 (1961) 1080.
[47] K.C. Janda, J.C. Hemminger, J.S. Winn, S.E. Novick, S.J. Harris and W. Klemperer, J. Chem. Phys. 63 (1975) 1419.
[48] M. Pierre, J. Phys. 36 (1975) 1095; 38 (1977) 39.